Available online at www.sciencedirect.com
SCIENCE DIRECT®
Journal of the Mechanics and Physics of Solids
54 (2006) 1862–1881
JOURNAL OF THE MECHANICS AND PHYSICS OF SOLIDS
www.elsevier.com/locate/jmps

Deformation of FCC nanowires by twinning and slip

Harold S. Park[a,*], Ken Gall[b], Jonathan A. Zimmerman[c]

[a]*Department of Civil and Environmental Engineering, Vanderbilt University, Nashville, TN 37235, USA*
[b]*School of Materials Science and Engineering, Georgia Institute of Technology, Atlanta, GA 30332, USA*
[c]*Sandia National Laboratories, Livermore, CA 94551, USA*

Received 14 September 2005; received in revised form 23 March 2006; accepted 25 March 2006

Abstract

We present atomistic simulations of the tensile and compressive loading of single crystal face-centered cubic (FCC) nanowires with ⟨1 0 0⟩ and ⟨1 1 0⟩ orientations to study the propensity of the nanowires to deform via twinning or slip. By studying the deformation characteristics of three FCC materials with disparate stacking fault energies (gold, copper and nickel), we find that the deformation mechanisms in the nanowires are a function of the intrinsic material properties, applied stress state, axial crystallographic orientation and exposed transverse surfaces. The key finding of this work is the first order effect that side surface orientation has on the operant mode of inelastic deformation in both ⟨1 0 0⟩ and ⟨1 1 0⟩ nanowires. Comparisons to expected deformation modes, as calculated using crystallographic Schmid factors for tension and compression, are provided to illustrate how transverse surface orientations can directly alter the deformation mechanisms in materials with nanometer scale dimensions.

Keywords: Nanowires; Atomistic simulations; Twinning; Slip; Stacking fault energy

1. Introduction

Nanowires have been studied intensely for nearly a decade due to their unique mechanical, electrical and optical properties that arise because of their nanometer size scale (Landman et al., 1990; Lieber, 2003; Yang, 2005). Metal nanowires have been found to exhibit unique physical behavior through a combination of theory, experiment and

*Corresponding author. Tel.: +1 615 936 7807; fax: +1 615 322 3365.
E-mail address: harold.park@vanderbilt.edu (H.S. Park).

0022-5096/$ - see front matter © 2006 Elsevier Ltd. All rights reserved.
doi:10.1016/j.jmps.2006.03.006

simulation. Examples of such phenomena are the ability of gold nanowires to form single atom chains under tensile loading (Mehrez and Ciraci, 1997; Rodrigues et al., 2000; Sanchez-Portal et al., 1999; Torres et al., 1999; Jagla and Tosatti, 2001; da Silva et al., 2001), quantized conduction through the single atoms chains (Ohnishi et al., 1998; Brandbyge et al., 1995), amorphization at high applied strain rates (Ikeda et al., 1999; Branicio and Rino, 2000), surface stress driven phase transformation of ⟨1 0 0⟩ gold nanowires (Diao et al., 2003; Gall et al., 2005), shape memory (Park et al., 2005; Park and Ji,) and pseudoelastic behavior (Park et al., 2005; Park and Ji, ; Liang and Zhou, 2005; Liang et al., 2005) of certain face-centered cubic (FCC) nanowires, stress-induced martensitic phase transformation of intermetallic nanowires (Park, 2006) and the formation of elongated stable nanobridges during the processing or tensile loading of ⟨1 1 0⟩ gold nanowires (Kondo and Takayanagi, 1997; Park and Zimmerman, 2006).

Atomistic, or molecular dynamics (MD) simulations of nanowires have been utilized to lend insight into the nanowire mechanical behavior and deformation mechanisms. In particular, researchers have utilized MD simulations to analyze the tensile failure modes in metal nanowires (Mehrez and Ciraci, 1997; Park and Zimmerman, 2006; Walsh et al., 2001; Park and Zimmerman, 2005; Wu et al., 2004; Gall et al., 2004; Liang and Zhou, 2004); one work which examined the yield behavior of nanowires in compression was that of Diao et al. (2004), who found a yield strength asymmetry in gold nanowires. The analysis of the failure modes of metal nanowires under different orientations has also been undertaken by only a few researchers (Mehrez and Ciraci, 1997; Park and Zimmerman, 2006; Coura et al., 2004), despite the experimental evidence which suggests a strong influence of crystallographic orientation on the structure and properties of metallic nanostructures (Kondo and Takayanagi, 1997).

In this work, we perform MD simulations to analyze the deformation of single crystal metal nanowires, with various crystallographic orientations loaded in tension and compression. Emphasis is placed on analyzing the propensity of the nanowires to deform by twinning and slip. The propensity for a bulk polycrystalline material to twin rather than slip depends primarily on the stacking fault energy of the material. In particular, materials with a low stacking fault energy may tend towards twinning (Meyers et al., 2002; El-Danaf et al., 1999; Christian and Mahajan, 1995; Chen et al., 2003) since the energetic penalty to forming a stacking fault during the nucleation and growth of a twin is minimized. Twins in FCC materials form through the nucleation and propagation of ⟨1 1 2⟩ partial dislocations on adjacent {1 1 1} planes. Since individual ⟨1 1 2⟩ partials can only move in one direction on close packed {1 1 1} planes, the resistance to twin formation in single crystals also depends strongly on the crystallographic orientation and applied stress state (tension versus compression) (Karaman et al., 2000). For example, in the ⟨1 0 0⟩ orientation deformed under compression, the leading ⟨1 1 2⟩ partial is more highly stressed relative to the trailing ⟨1 1 2⟩ partial, leading to easy twin formation. In the ⟨1 0 0⟩ orientation deformed under tension, the trailing ⟨1 1 2⟩ partial is more highly stressed relative to the leading ⟨1 1 2⟩ partial, suppressing partial dislocation nucleation and twin formation. The situation is reversed in the ⟨1 1 0⟩ orientation; twinning is favored under tension and not under compression. The aforementioned issues pertain to bulk single crystals and will have some relevance to single crystal nanowires. However, other issues, such as surface orientation, surface stresses and stacking fault energies may also influence the propensity of a nanowire to deform by slip or twinning.

The MD simulations performed in this work thus utilize three different FCC materials (copper, nickel and gold) with disparate stacking fault energies to analyze the deformation behavior under tension and compression along the ⟨1 0 0⟩ and ⟨1 1 0⟩ orientations. The different stress states and orientations are selected because they bias the relative resistance of twinning and slip in the various materials from a crystallographic standpoint. The importance of accurately modeling stacking fault energies when studying inelasticity in gold nanowires was recently shown by Park and Zimmerman (2005, 2006). The spread in stacking fault energies facilitates a thorough investigation into the mechanisms of twinning and slip in FCC metal nanowires.

We begin this paper by discussing the simulation methods used in this work. We next present the results of the numerical simulations concentrating on the different deformation modes observed in the various materials depending on the loading condition, wire orientation and side surface orientations. After presenting the numerical predictions, we discuss the fundamental mechanisms controlling the deformation in the nanowires. Special emphasis is placed on the unique role that side surface orientations have in controlling the operant deformation mechanisms in the nanometer scale wires. Finally, we end the paper with concluding remarks.

2. Simulation methods

The MD simulations performed in this work used the embedded atom method (EAM) (Daw and Baskes, 1984) as the underlying atomic interaction model. For the EAM, the total energy U for a system of atoms can be written as

$$U = \sum_{i}^{N} \left(F_i(\bar{\rho}_i) + \frac{1}{2} \sum_{j \neq i}^{N} \phi_{ij}(R_{ij}) \right), \tag{1}$$

where the summations in (1) extend over the total number of atoms N in the system, F_i is the embedding function, $\bar{\rho}_i$ is the electron density at atom i, ϕ_{ij} is a pair interaction function and R_{ij} is the distance between atoms i and j.

We utilized the Angelo–Moody–Baskes EAM potential (Angelo et al., 1995) to model nickel, while copper and gold were modeled using two different EAM potentials of Foiles (Park and Zimmerman, 2005); these potentials were chosen because they accurately model the material stacking fault energies (Zimmerman et al., 2000). Moreover, these three materials were selected as they have fairly disparate stacking fault energies; the spread in stacking fault energies will allow us to study the impact of the stacking fault energies on the deformation mechanisms for various wire orientations and stress states. The relevant potential parameters for surface and stacking fault energies are summarized in Table 1.

Four different nanowire orientations were utilized in this study as schematically shown in Fig. 1. The ⟨1 0 0⟩/{1 0 0} nanowire has a ⟨1 0 0⟩ longitudinal orientation with four {1 0 0} side surfaces. The ⟨1 0 0⟩/{1 1 0} has a ⟨1 0 0⟩ longitudinal orientation with four {1 1 0} side surfaces. The ⟨1 1 0⟩ nanowire has a ⟨1 1 0⟩ longitudinal orientation with two {1 1 0} side surfaces and two {0 0 1} side surfaces. The ⟨1 1 0⟩/{1 1 1} nanowire has a ⟨1 1 0⟩ longitudinal orientation with four {1 1 1} side surfaces. Of these four nanowire orientations, three have been experimentally observed: ⟨1 0 0⟩/{1 0 0} (Rodrigues et al., 2000; Kondo and Takayanagi, 1997), ⟨1 1 0⟩ (Rodrigues et al., 2000; Kondo and Takayanagi, 1997), and ⟨1 1 0⟩/{1 1 1} (Gulseren et al., 1998; Kondo and Takayanagi, 2000; Liu et al., 2003). The

Table 1
Comparison of relevant energetic ratios for EAM potentials of nickel, copper and gold. Surface and stacking fault energies are all in units of mJ/m^2

Material	γ_{sf}	γ_{usf}	γ_{100}	γ_{111}	$\gamma_{111}/\gamma_{100}$	γ_{usf}/γ_{sf}
Gold (EAM)	32	92	1090	1180	0.924	2.88
Gold (Exp)	32		1283	1627	0.79	
Copper (EAM)	39	133	1351	1452	0.930	3.43
Copper (Exp)	45		1952	2166	0.90	
Nickel (EAM)	125	264	1928	2060	0.936	2.11
Nickel (Exp)	125		2011	2426	0.83	

The second line for each material contains stacking fault energies from Hirthe and Lothe (1982) and surface energies from Vitos et al. (1998).

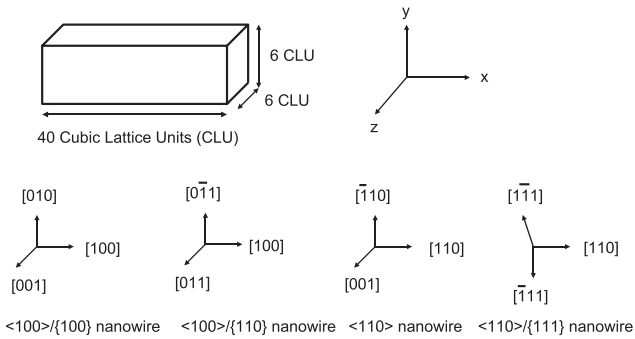

Fig. 1. Schematic of nanowire sizes, crystallographic orientations and transverse directions considered in this paper.

$\langle 1\,0\,0\rangle/\{1\,1\,0\}$ wire has to-date not been synthesized experimentally, and thus serves as a theoretical example to help illustrate the effects of size surface orientation on the observed deformation mechanism in the nanowires.

The $\langle 1\,0\,0\rangle/\{1\,0\,0\}$, $\langle 1\,0\,0\rangle/\{1\,1\,0\}$ and $\langle 1\,1\,0\rangle$ square cross section nanowires were created by extracting a rectangular wire from a bulk FCC crystal. The wire lengths were all 40 cubic lattice units in the x-direction, with cross sectional lengths of six cubic lattice units in the y- and z-directions as shown in Fig. 1. The $\langle 1\,0\,0\rangle/\{1\,0\,0\}$, $\langle 1\,0\,0\rangle/\{1\,1\,0\}$ and $\langle 1\,1\,0\rangle$ wires were first relaxed using conjugate gradient energy minimization. The gold wires were then equilibrated at 50 K while the copper and nickel wires were equilibrated at 300 K using a Nosé–Hoover thermostat (Nosé, 1984; Hoover, 1985) for 20 ps, then loaded in tension or compression in the x-direction using a uniform strain loading condition without thermostatting to ensure adiabatic loading conditions. The uniform strain loading condition was applied by fixing one end of the wire, then applying velocities to atoms along the loading direction that vary linearly from zero at the fixed end to a maximum value at the free end; while the strain rate due to this loading condition is high ($\dot{\varepsilon} \approx 10^9$) as is typical for MD simulations, this loading condition is typically utilized in the literature to mitigate shock wave loading effects on nanowire deformation. The different equilibration temperatures were chosen to be less than the critical reorientation temperature at which

⟨1 0 0⟩/{1 0 0} nanowires have been found to reorient to ⟨1 1 0⟩ nanowires with {1 1 1} surfaces for a given material (Park et al., 2005; Liang and Zhou, 2005).

The ⟨1 1 0⟩/{1 1 1} nanowires were created from ⟨1 0 0⟩ nanowires extracted from the bulk. The wire ends were constrained to move only in the z-direction, then the atoms were thermalized by using a velocity rescaling algorithm. Upon application of a critical amount of thermal energy (Park et al., 2005; Liang and Zhou, 2005), the nanowires begin to contract in the z-direction, eventually reorienting to a ⟨1 1 0⟩/{1 1 1} configuration. The ⟨1 1 0⟩/{1 1 1} wires have a rhombic cross section with four {1 1 1} surfaces in contrast to the ⟨1 1 0⟩ wires which have a square cross section and {0 0 1} and {1 1 0} surfaces as seen in Fig. 1. After reorientation was completed, the nanowires were loaded in both tension and compression in the z-direction by application of a uniform strain loading condition without thermostatting to ensure adiabatic loading conditions. The equations of motion were integrated in time using a velocity Verlet algorithm, and all simulations were performed using the Sandia-developed code Warp (Plimpton, 1995; Warp, ; Horstemeyer et al.,). Periodic boundary conditions were not used at any time for any of the simulations in this work.

3. Simulation results

3.1. *Tension of* ⟨1 0 0⟩/{1 0 0} *nanowires*

The tensile deformation of metal nanowires, particularly from the ⟨1 0 0⟩/{1 0 0} orientation has been frequently studied in the literature. Examples of these studies can be found in the following references (Mehrez and Ciraci, 1997; Park and Zimmerman, 2005; Wu et al., 2004; Gall et al., 2004; Liang and Zhou, 2004). In general, ⟨1 0 0⟩/{1 0 0} nanowires deformed under tension show yield and plasticity associated with both full and partial dislocation nucleation and propagation. Because of the abundance of prior work on this orientation, we focus on other orientations and loading conditions.

3.2. *Compression of* ⟨1 0 0⟩/{1 0 0} *nanowires*

In this section, we present numerical simulations of the compression of the ⟨1 0 0⟩/{1 0 0} nanowires. Snapshots of the deformation process can be seen in Fig. 2 for the nickel nanowire. As can be seen, the ⟨1 0 0⟩/{1 0 0} wire accommodates the compressive loading by the formation of multiple twins within the nanowire interior. The twinning also results in the exposure of low energy {1 1 1} surfaces on the deformed wire rather than the original {1 0 0} surfaces. The new {1 1 1} surfaces are created as a result of the crystallography of twinning and the relative orientation of the original wire surfaces with respect to the twinned wire surfaces. The ability of the twins to result in a reduction of surface energy provides additional driving force for twinning relative to other deformation modes, such as plasticity through full dislocation motion (which results in higher energy surface steps) or distributed partial dislocation defects and stacking faults.

Gold and copper nanowires are also found to exhibit twinning during the compression of ⟨1 0 0⟩/{1 0 0} nanowires, indicating that the difference in stacking fault energy does not alter the operant deformation mechanism for wires compressed in the ⟨1 0 0⟩ direction. Instead, the favorable orientation of twinning planes and directions, coupled with surface

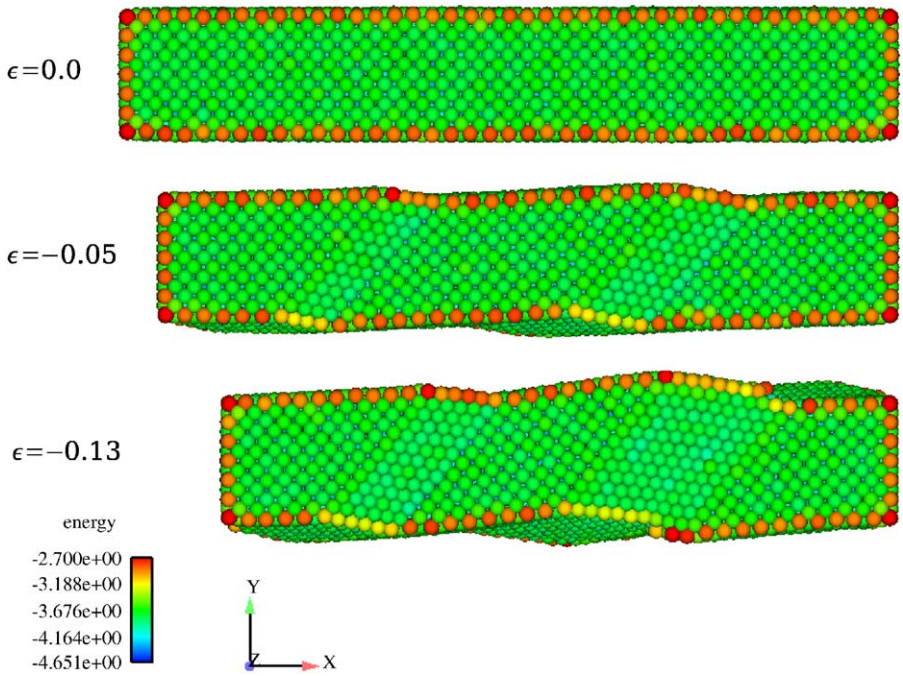

Fig. 2. Twinning during the compression of a ⟨1 0 0⟩/{1 0 0} nickel nanowire. The potential energy values are in eV.

energy reduction imparted by deformation twinning, dominates all other energetic barriers for ⟨1 0 0⟩/{1 0 0} nanowire compression.

3.3. *Compression of* ⟨1 0 0⟩/{1 1 0} *nanowires*

We present in this section numerical simulations of the compression of the ⟨1 0 0⟩/{1 1 0} nanowires. This nanowire has the same ⟨1 0 0⟩ longitudinal orientation as the ⟨1 0 0⟩/{1 0 0} wires discussed in Section 3.2, but with the crystal rotated about its longitudinal axis by 45° such that the exposed side surfaces are of the {1 1 0} type.

As can be seen in Fig. 3, the copper ⟨1 0 0⟩/{1 1 0} wire shows parallel stacking fault structures during compressive deformation with spatially distributed stacking faults. Of particular interest, the stacking faults occur on two variants at different sections along the wire, as illustrated in the top and bottom set of images in Fig. 3. In this and subsequent figures, we illustrate the deformation in the nanowires using the centrosymmetry parameter (Kelchner et al., 1998), which is a measure of local atomic coordination; a value of zero indicates a fully coordinated, bulk atom.

Gold and nickel showed similar behavior in compression for the ⟨1 0 0⟩/{1 1 0} orientation. Interestingly, the ⟨1 0 0⟩/{1 1 0} wires do not show twinning as observed in the ⟨1 0 0⟩/{1 0 0} wires discussed above, even though the wires differ only by a rotation about the wire axis. This observation will be explained further in the Discussion section of this paper.

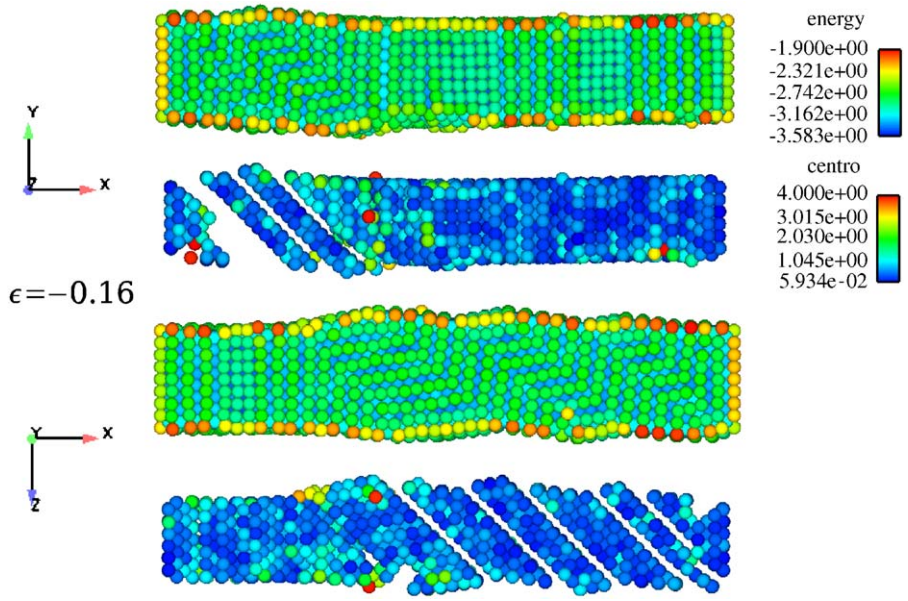

Fig. 3. Parallel stacking fault structure during the compression of a ⟨1 0 0⟩/{1 1 0} copper nanowire. The top image for each orientation corresponds to potential energy in eV; the bottom image for each orientation shows atoms highlighted by the centrosymmetry parameter (Kelchner et al., 1998).

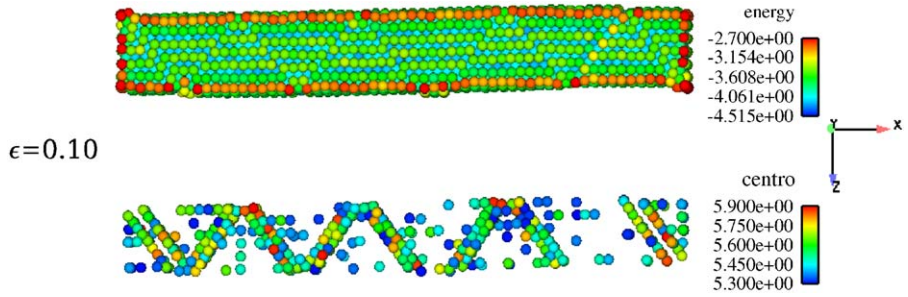

Fig. 4. Top: snapshot at strain of $\varepsilon = 0.10$ during tensile loading of a ⟨1 1 0⟩ nickel nanowire. Values of potential energy in eV are shown. Bottom: stacking faults at same strain level, indicating a slip dominated process. Values are in terms of the centrosymmetry parameter (Kelchner et al., 1998).

3.4. *Tension of* ⟨1 1 0⟩ *nanowires*

In this section, we present numerical simulations of the tensile loading of ⟨1 1 0⟩ nanowires. Snapshots of the deformation process can be seen in Fig. 4 for nickel. The predominant deformation mechanism is slip via partial dislocation nucleation; this is evident by the stacking faults observed along {1 1 1} planes in Fig. 4. Copper ⟨1 1 0⟩ nanowires are found to behave similarly in tension, with stacking faults caused by the nucleation and propagation of partial dislocations.

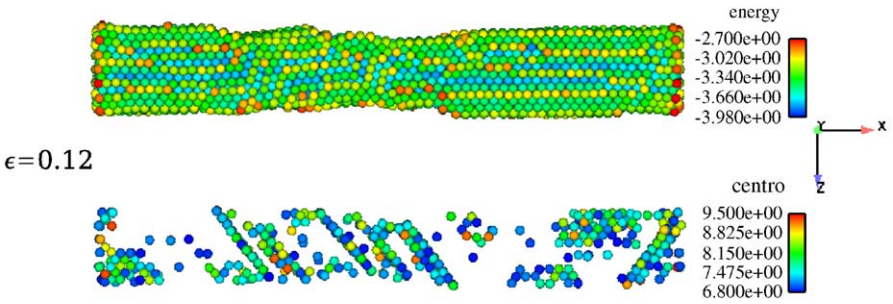

Fig. 5. Top: snapshot at strain of $\varepsilon = 0.12$ during tensile loading of a $\langle 1\,1\,0\rangle$ gold nanowire. Values of potential energy in eV are shown. Bottom: snapshot of parallel stacking fault structure at the same strain level. Values are in terms of the centrosymmetry parameter (Kelchner et al., 1998).

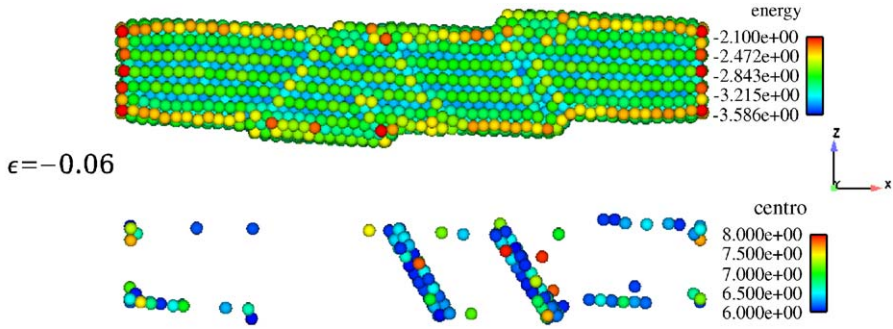

Fig. 6. Snapshots of the slip-dominated deformation process at a compressive strain of $\varepsilon = -0.06$ during the compression of $\langle 1\,1\,0\rangle$ copper nanowires. The potential energy values are in eV, while the centrosymmetry is modeled according to Kelchner et al. (1998).

In contrast, gold $\langle 1\,1\,0\rangle$ nanowires show a slightly different type of defect structure under tensile loading. A snapshot of the gold $\langle 1\,1\,0\rangle$ wire is shown in Fig. 5. Unlike copper and nickel, gold $\langle 1\,1\,0\rangle$ nanowires show a parallel (single variant) stacking fault structure during tensile deformation. The parallel stacking fault arrangement in the gold wires is twinning-like, although adjacent stacking faults did not join together to form twins. The major difference between the $\langle 1\,0\,0\rangle/\{1\,0\,0\}$ wires deformed in compression and the $\langle 1\,1\,0\rangle$ wires deformed in tension was the distribution of the stacking fault defects. In the $\langle 1\,0\,0\rangle/\{1\,0\,0\}$ wires, the stacking faults occurred on adjacent planes leading to definitive twin formation, while the stacking fault formation in the tensile loaded $\langle 1\,1\,0\rangle$ wires was distributed throughout the wire without the formation of twins.

3.5. *Compression of* $\langle 1\,1\,0\rangle$ *nanowires*

In this section, we present simulations of the compression of $\langle 1\,1\,0\rangle$ nanowires. Snapshots of the deformation process in the copper nanowire can be seen in Fig. 6. In comparison to the $\langle 1\,0\,0\rangle/\{1\,0\,0\}$ oriented nanowires, twinning is not observed during the compression of the $\langle 1\,1\,0\rangle$ nanowires. Instead, the compressive deformation is accommodated by the formation and propagation of both full $\langle 1\,1\,0\rangle/\{1\,1\,1\}$ and partial

dislocations; this is illustrated in Fig. 6 for the copper nanowire, which shows the surface steps created by the propagation of full dislocations as well as the stacking faults created by the partials.

Gold and nickel also showed similar defect structures during ⟨1 1 0⟩ compression, as both nanowires exhibited a combination of partial and full dislocations in response to the compressive loading. Nickel showed the smallest number of partial dislocations and stacking faults in ⟨1 1 0⟩ compression, commensurate with its high stacking fault energy. Twinning was not observed in any of the ⟨1 1 0⟩ wires deformed under compression.

3.6. *Compression of* ⟨1 1 0⟩/{1 1 1} *nanowires*

We now present results from the compression of ⟨1 1 0⟩/{1 1 1} nanowires. This wire differs from the ⟨1 1 0⟩ wires in Sections 3.4 and 3.5 since it possesses low energy {1 1 1} side surfaces and a rhombic rather than square cross section. Snapshots of the deformation for the nickel nanowire can be seen in Fig. 7, which shows both the wire potential energy and centrosymmetry (Kelchner et al., 1998), respectively. During the compression of the ⟨1 1 0⟩/{1 1 1} nanowires, there is a noticeable absence of dislocation line defects within the nanowire interior; this is illustrated by showing only those atoms that are not fully coordinated via their centrosymmetry value, as in Fig. 7.

Instead, the wire cross section remains unchanged, and atoms begin piling up around the fixed edges of the nanowire to accommodate the lack of line defects nucleating from the

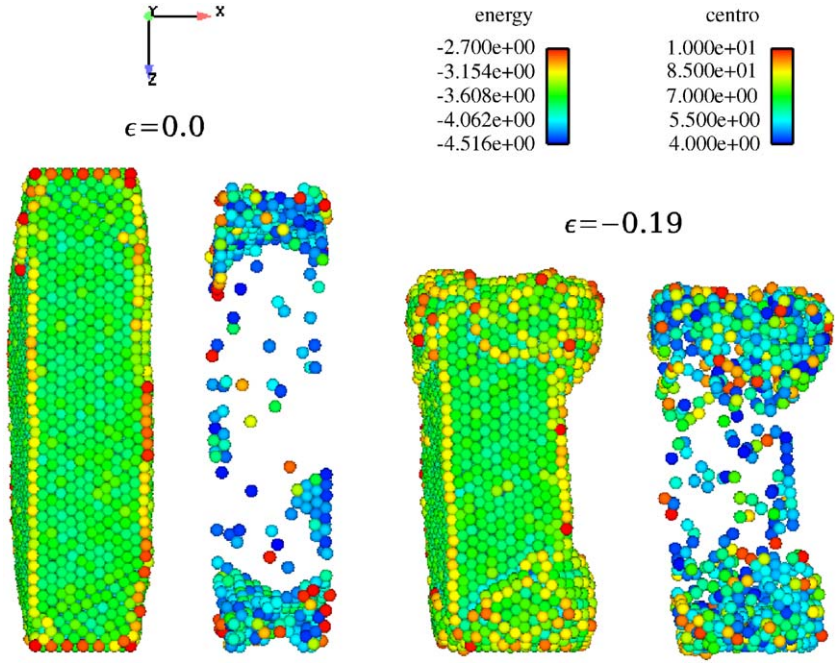

Fig. 7. Compression of a ⟨1 1 0⟩/{1 1 1} nickel nanowire. The images at each time can be decomposed as (left): potential energy values in eV, (right): centrosymmetry parameter (Kelchner et al., 1998). Centrosymmetry is shown to highlight the defect-free interior of the nickel nanowire.

initially low energy surfaces of the wire. The lack of defects forming in the wire interior indicates that the ⟨1 1 0⟩/{1 1 1} configuration is energetically stable, and supports the notion that surface energy reduction is a key component to nanowire *mechanical* stability. The compression was continued until a strain of about 19% relative to the original reoriented ⟨1 1 0⟩/{1 1 1} configuration. The compressive deformation mechanism in the ⟨1 1 0⟩/{1 1 1} wires in Fig. 7 differs considerably compared to the compressive deformation mechanism in the ⟨1 1 0⟩ wires seen in Fig. 6 even though these wires share the same longitudinal orientation.

3.7. *Tension of* ⟨1 1 0⟩/{1 1 1} *nanowires*

We also considered the tensile loading of ⟨1 1 0⟩/{1 1 1} nanowires. Recent work has demonstrated that both shape memory (Park et al., 2005) and pseudoelastic behavior (Park et al., 2005; Liang and Zhou, 2005) is observed in certain FCC materials when loaded in tension from this initial configuration (Park et al., 2005; Liang and Zhou, 2005). We illustrate the deformation process starting with a ⟨1 1 0⟩/{1 1 1} copper nanowire in Fig. 8. Upon application of tensile loading to the ⟨1 1 0⟩/{1 1 1} nanowire, two twins nucleate at opposing ends of the wire. Upon continued tensile loading, the twin boundaries eventually propagate towards each other, and then annihilate, leaving a pristine ⟨1 0 0⟩ nanowire as seen at a strain of $\varepsilon = 0.43$ in Fig. 8.

The full reorientation back to the initial ⟨1 0 0⟩/{1 0 0} wire is seen in nickel and copper, but not gold. For all materials, the reorientation back to ⟨1 0 0⟩/{1 0 0} begins with the nucleation of twins at opposing ends of the nanowire. However, it was determined in previous work by the current authors (Park et al., 2005) that the formation of {1 1 1} interior stacking faults within the twins for gold prevented the full reorientation back to ⟨1 0 0⟩/{1 0 0} from occurring. Interior stacking faults were observed in nickel and copper, which reorient back to the initially defect free ⟨1 0 0⟩ orientation from ⟨1 1 0⟩/{1 1 1}. The tensile deformation mechanism in the ⟨1 1 0⟩/{1 1 1} wires shown in Fig. 8 differs

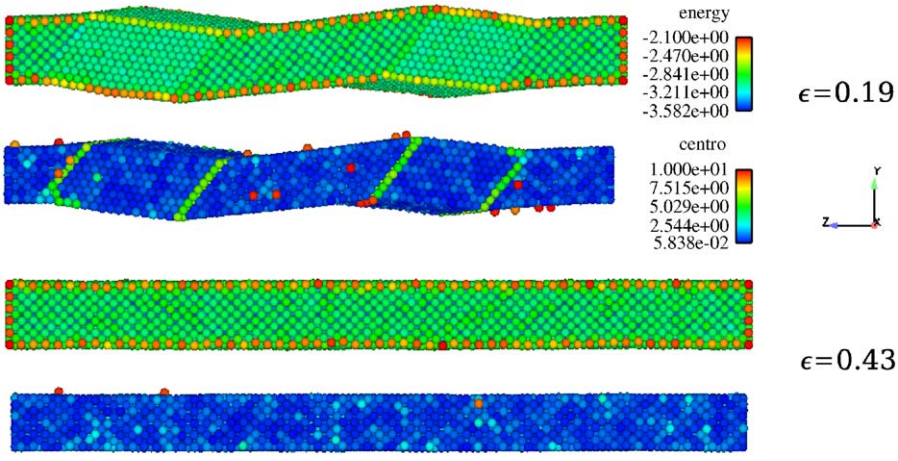

Fig. 8. Tensile loading of the initially ⟨1 1 0⟩/{1 1 1} copper nanowire. The top image at each time correspond to potential energy in eV; the bottom image at each time shows atoms highlighted by the centrosymmetry parameter (Kelchner et al., 1998).

considerably compared to the tensile deformation mechanism in the ⟨1 1 0⟩ wires seen in Figs. 4 and 5.

4. Discussion

We now discuss the deformation modes observed through the MD simulations for the nanowires of various materials, crystallographic orientations and applied stress states. To assist in the interpretation of the results, we calculated Schmid factors for the ⟨1 0 0⟩ and ⟨1 1 0⟩ orientations for slip of full dislocations, tensile-induced twinning (partial dislocation slip) and compression-induced twinning (partial dislocation slip). The Schmid factor is a measure of the crystallographic likelihood of observing either twinning or slip for a given orientation and stress state, where 0.5 is a maximum value and 0.0 indicates that the deformation mode is geometrically impossible for a given orientation and stress state. Schmid factors represent the maximum resolved shear stress factor for all possible slip/twin plane and slip/twin direction combinations. The resolved shear stress factor times the uniaxial applied stress provides the resolved shear stress across a particular slip/twin plane and slip/twin direction. Thus, the Schmid factors are purely geometric, or crystallographically-dependent constants that are independent of material properties.

The Schmid factors, which were calculated following the works of Karaman et al. (2001a, b), are presented in Table 2. Typically the Schmid factor is used to analyze the response of bulk, polycrystalline materials; in the deformation of nanowires, other factors such as surface stresses and transverse orientations need to be considered, as will be demonstrated herein. Thus when discussing the Schmid factor analysis, we will refer to general ⟨1 0 0⟩ and ⟨1 1 0⟩ orientations without regard for surface orientation as those are not included in the Schmid factor calculations. From a crystallographic standpoint, partial dislocation motion and twinning would be favored in compressed ⟨1 0 0⟩ wires and tensile loaded ⟨1 1 0⟩ wires as seen in Table 2. On the other hand, partial dislocation motion is relatively difficult in compressed ⟨1 1 0⟩ wires and tensile loaded ⟨1 0 0⟩ wires, potentially favoring the motion of full dislocations, which have higher energy but also more favorable crystallographic alignment (i.e. higher Schmid factors as seen in Table 2).

We begin by discussing the compression of the ⟨1 0 0⟩/{1 0 0} wires. In the ⟨1 0 0⟩/{1 0 0} orientation, nickel, copper and gold all demonstrated twinning during the compressive loading. The Schmid factor data from Table 2 indicates that twinning in compression is crystallographically favored over pure slip for a general ⟨1 0 0⟩ orientation. Equally as important, twinning in compression allows the nanowires to reduce their surface energies by exposing lower energy {1 1 1} surfaces instead of the initial {1 0 0} surfaces. For FCC metals, this surface energy reduction has been experimentally observed to be on the order of 20% (Wan et al., 1999). In contrast, the EAM potentials utilized in this work show

Table 2
Schmid factors for various wire orientations considering slip (full dislocations), tensile-induced twinning (partial dislocation slip) and compression-induced twinning (partial dislocation slip)

Orientation	Slip	Tensile-twin	Compression-twin
⟨1 0 0⟩	0.42	0.24	0.47
⟨1 1 0⟩	0.41	0.48	0.25

between a 6% and 7% decrease in surface energies between the {1 0 0} and {1 1 1} surfaces, though these potentials more accurately capture surface energies than previous EAM potentials (Foiles et al., 1986). While EAM potentials are well-known to underpredict the surface energies of FCC metals (Shenoy, 2005), the combination of the creation of low energy surfaces and the favorable orientation of twin planes provides a strong driving force for ⟨1 0 0⟩/{1 0 0} FCC nanowires to twin under compression. We do not discuss tension of the ⟨1 0 0⟩/{1 0 0} wires due to the extensive literature on this orientation (Mehrez and Ciraci, 1997; Park and Zimmerman, 2005; Wu et al., 2004; Gall et al., 2004; Liang and Zhou, 2004) which clearly demonstrates that slip is preferred for that orientation and applied stress state.

The effects of free surfaces on the deformation modes seen in nanowires is first seen by comparing the compressive deformation of ⟨1 0 0⟩/{1 0 0} and ⟨1 0 0⟩/{1 1 0} wires, which have identical ⟨1 0 0⟩ normal orientations but different side surfaces. Note that standard crystallographic arguments (Schmid factors) would predict the same deformation mode for all ⟨1 0 0⟩ wires as transverse surface orientations are not considered. For a twin to grow, partial dislocations must move on the same crystallographic variant of adjacent twinning planes. In the ⟨1 0 0⟩/{1 0 0} wires, twinning can result in the formation of two low energy {1 1 1} side surfaces, so it is the favored deformation mechanism and partial dislocations move on adjacent planes to effectively grow the twin. On the other hand, in the ⟨1 0 0⟩/{1 1 0} wires, twins are incapable of forming low energy {1 1 1} side surfaces, thus one of the driving forces for twinning is reduced, and twins are not observed. Rather, in the ⟨1 0 0⟩/{1 1 0} wires, partial dislocations move on multiple crystallographic variants causing dispersed stacking faults with various orientations as illustrated in Fig. 3. Since the ⟨1 0 0⟩/{1 0 0} and ⟨1 0 0⟩/{1 1 0} wires are identical besides transverse surface orientations, the difference in their operant deformation mechanism demonstrates the importance of free surface characteristics on nanowire deformation.

The ⟨1 1 0⟩ wires deformed under tension also have a high Schmid factor for the motion of partial dislocations and the formation of twins, similar to the compressed wires with ⟨1 0 0⟩ orientations. The Schmid factor for the motion of full dislocations is slightly lower than the Schmid factor for twinning as seen in Table 2. Although the tensile loaded ⟨1 1 0⟩ wires demonstrated the formation of stacking faults, twins did not form from these stacking faults, which is fundamentally different than the compressed ⟨1 0 0⟩/{1 0 0} wires or the tensile loaded ⟨1 1 0⟩/{1 1 1} wires to be discussed later. The reason for this difference is the crystallography of the side surfaces, which in bulk materials is not critical. For example, in the compressed ⟨1 0 0⟩/{1 0 0} wires, twinning causes the exposure of low energy {1 1 1} surfaces, which is favored over the formation of randomly dispersed stacking faults caused by partial dislocation motion. However, the tensile loaded ⟨1 1 0⟩ wires cannot form low energy {1 1 1} side surfaces due to twinning because of crystallographic constraints. Consequently, the formation of twins (which requires the nucleation of sequential partial dislocations on adjacent planes) is not sufficiently energetically favorable compared to dispersed stacking faults and thus the latter is observed inthe tensile loaded ⟨1 1 0⟩ wires.

During the compression of the ⟨1 1 0⟩ nanowires, the Schmid factor analysis indicates that slip of full dislocations would be crystallographically preferred compared to twinning. The MD simulations confirm this trend; all three materials plastically deform via the nucleation of both full and partial dislocations. Partial dislocations and stacking faults are still observed, despite their unfavorable crystallographic alignment in compressed ⟨1 1 0⟩

nanowires, because of the lower relative energy of this deformation mechanism compared to slip of full dislocations. Interestingly, the stacking fault energies of the materials seem to correlate with the deformation seen for this orientation and stress state; nickel nanowires, which have a stacking fault energy three to four times either copper or gold, possess a significantly lower density of stacking faults and partial dislocations as compared to either copper and gold, which both have lower stacking fault energies. A final comment concerns the effect of surface energies; {1 1 0} surfaces are typically the highest energy surface for FCC metals, higher than the {1 0 0} surfaces which were shown to change into {1 1 1} surfaces under tensile loading of certain orientations. Due to crystallographic constraints, the {1 1 0} surfaces are not able to lower their energy by conversion to {1 0 0} or {1 1 1} surfaces under either tensile or compressive loading for the ⟨1 1 0⟩ wires with square cross sections and the orientations shown in Fig. 1.

Stress–strain curves for all materials loaded in tension and compression of the ⟨1 1 0⟩ nanowires are shown in Figs. 9 and 10. Under both loading directions, nickel has the highest yield strength, followed by copper then gold. Due to the different deformation mechanisms operating under tension versus compression as well as the effect of tensile surface stresses, all materials exhibit yield strength asymmetry to varying degrees; this was seen in ⟨1 0 0⟩ and ⟨1 1 1⟩ gold nanowires by Diao et al. (2004). For example, gold shows the largest difference in yield strain between tension ($\varepsilon = 0.67$) and compression ($\varepsilon = -0.42$). However, nickel shows the largest yield stress differential being much stronger in compression ($\sigma_{xx} = -12.39\,\text{GPa}$) than in tension ($\sigma_{xx} = 7.79\,\text{GPa}$). The yield strain asymmetry can be explained by the fact that gold has the largest ⟨1 1 0⟩ surface stress (Wan et al., 1999); because of this, the gold nanowires will have larger intrinsic lattice strains, leading to the yield strain asymmetry. The yield stress asymmetry is driven by the energy barrier and crystallography of different inelastic deformation mechanisms observed in tension versus compression. For example, under compression, the ⟨1 1 0⟩ wires are forced

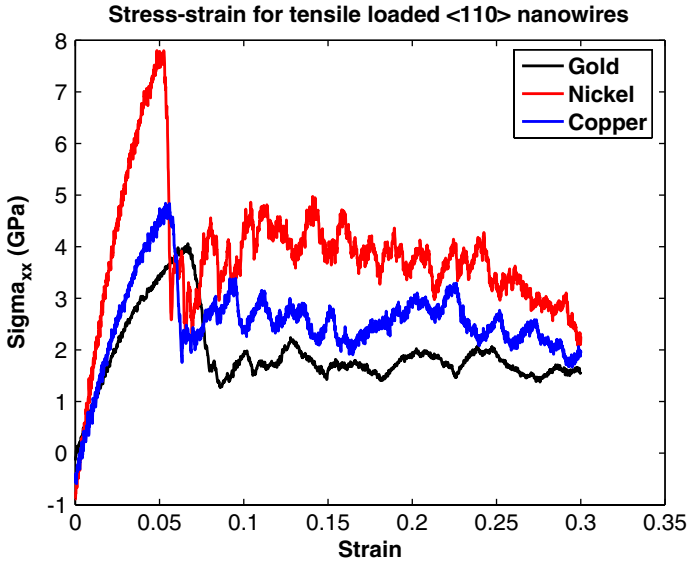

Fig. 9. Stress–strain curves for ⟨1 1 0⟩ nanowires loaded in tension.

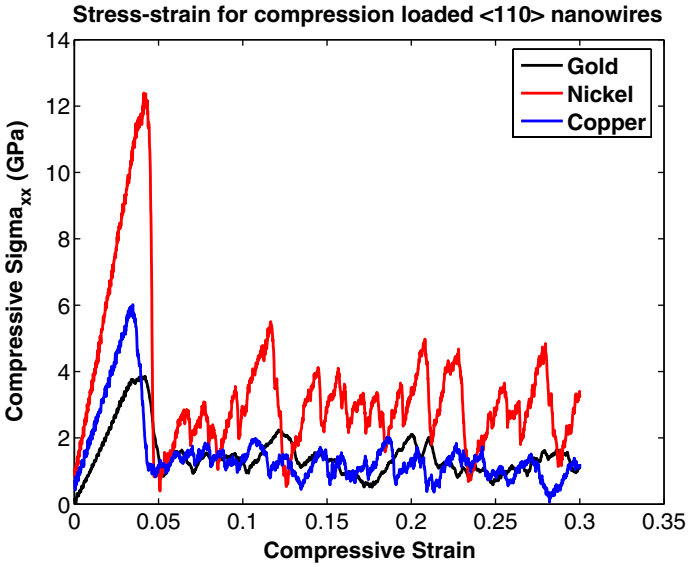

Fig. 10. Stress–strain curves for ⟨1 1 0⟩ nanowires loaded in compression.

to deform by relatively high-energy full dislocation motion because low energy partial dislocation motion is not crystallographically favored, leading to high strength levels. On the other hand, under tension, the ⟨1 1 0⟩ wires deform by low-energy partial dislocation motion, which is crystallographically favored and leads to lower stress levels at the onset of inelastic deformation.

The ⟨1 1 0⟩/{1 1 1} nanowire demonstrates various interesting responses. First, it has been shown in previous works that nanowires with this orientation can exhibit both shape memory (Park et al., 2005) and pseudoelastic behavior (Park et al., 2005; Liang and Zhou, 2005). Secondly, this orientation contains only low energy {1 1 1} side surfaces prior to loading. By compressing the ⟨1 1 0⟩/{1 1 1} wire, we discovered that even up to fairly large strains of 19%, the wire interior remained line defect free. Instead, an end effect dominated crushing-type deformation mode is observed, in which atoms on the {1 1 1} surfaces are driven to form clumps of atoms surrounding the wire ends, while the wire interior remains defect free. Because line defects tend to nucleate at the surfaces of nanostructured materials deformed under uniaxial loading, these simulations indicate that the low energy {1 1 1} surfaces act to prevent defect nucleation from critically stressed surface sites. It is important to emphasize that compressed ⟨1 1 0⟩ wires without low energy {1 1 1} side surfaces experience plastic flow by partial and full dislocation motion as shown in Fig. 6 while the compressed ⟨1 1 0⟩ wires with low energy surfaces are resilient to inelastic deformation via slip or twinning as shown in Fig. 7. Such an effect would never be observed in bulk materials, since this implies that the exposed side surface orientation has a first order influence on the operant deformation mechanism and the strength of the crystal.

The ⟨1 1 0⟩/{1 1 1} wires show a different behavior in tension. As was discussed earlier, ⟨1 0 0⟩/{1 0 0} wires can reorient into ⟨1 1 0⟩/{1 1 1} wires by the creation and propagation of twins. We find that under reversed tensile loading, the reverse is not always true; nickel and copper can regain their initial ⟨1 0 0⟩/{1 0 0} configuration through the reversal of the

twins, while gold cannot. The reason for this can be tied to the low stacking fault energy of gold; it has been shown (Park et al., 2005) that the twins formed during the ⟨1 0 0⟩/{1 0 0} to ⟨1 1 0⟩/{1 1 1} reorientation do not have defect free interiors as those formed in nickel and copper do. Instead, the twins formed in gold contain interior {1 1 1} stacking faults, which are not reversible under tensile loading. The low stacking fault energy of gold allows the creation of complex defect structures which prevent reversibility as seen in copper and nickel. This reversibility of defect-free twins allows copper and nickel to exhibit shape memory and pseudoelastic behavior (Park et al., 2005), while gold cannot. It is also interesting that the tensile loaded ⟨1 1 0⟩/{1 1 1} wires show twins while the tensile loaded ⟨1 1 0⟩ wires show distributed stacking faults for nickel and copper. Again, crystallographic constraints caused by the transverse surface orientations and associated surface energy values strongly influence the operant deformation mode of the nanowire. In particular, twinning in the ⟨1 1 0⟩/{1 1 1} wires leads to the formation of clean {1 0 0} surfaces. In contrast, twinning cannot lead to the formation of such surfaces in the ⟨1 1 0⟩ wires that do not have initial {1 1 1} faces, thus distributed stacking faults are observed and pseudoelastic and shape memory behavior are not observed.

The stress–strain response for the ⟨1 1 0⟩/{1 1 1} wires loaded in compression is shown in Fig. 11. In comparison to the ⟨1 1 0⟩ wires in compression, the ⟨1 1 0⟩/{1 1 1} wires show similar compressive behavior, in that there appears to be a yield point which for both copper and gold is lower than the ⟨1 1 0⟩ wires and which is similar for nickel. The yield stress is however significantly lower for the ⟨1 1 0⟩/{1 1 1} wires. We should also re-emphasize here that while the ⟨1 1 0⟩/{1 1 1} wires show yield on the stress–strain curve in compression, the interior of the wires as illustrated in Fig. 7 are defect free. Instead, yield for the ⟨1 1 0⟩/{1 1 1} wires occurs at the ends of the wires, where atoms begin to clump around the edges in response to the compressive loading.

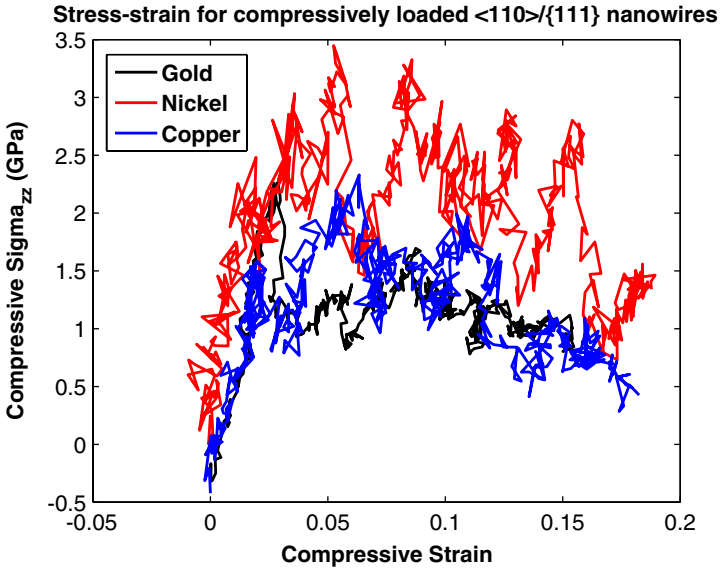

Fig. 11. Stress–strain curves for ⟨1 1 0⟩/{1 1 1} nanowires loaded in compression.

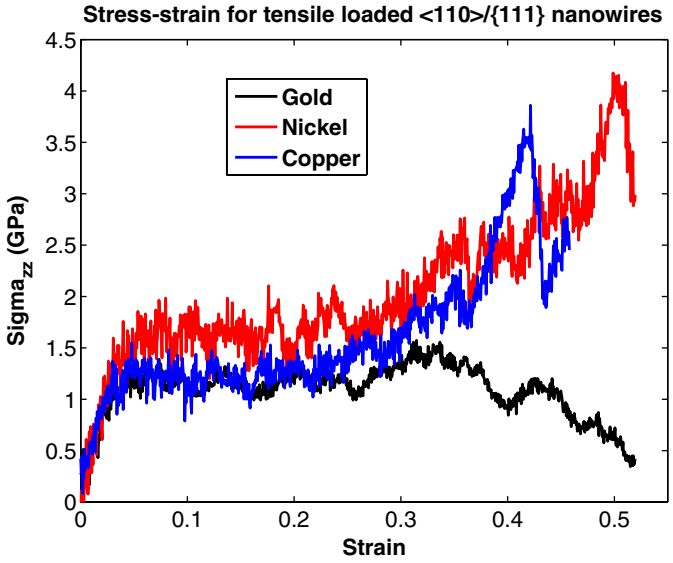

Fig. 12. Stress–strain curves for ⟨1 1 0⟩/{1 1 1} nanowires loaded in tension.

The stress–strain curves for the ⟨1 1 0⟩/{1 1 1} wires loaded in tension is shown in Fig. 12. As can be seen, nickel and copper show strains of nearly 40% while reorienting back to the original ⟨1 0 0⟩/{1 0 0} configuration. This strain is recoverable upon unloading and/or heating and is significantly larger than recoverable strains measured in standard shape memory alloys such as NiTi, which are on the order of 10%. This recoverable strain endows copper and nickel nanowires with unique shape memory (Park et al., 2005) and pseudoelastic (Park et al., 2005; Liang and Zhou, 2005) behavior. In contrast, the gold nanowires yield at about 30% strain before complete reorientation back to ⟨1 0 0⟩ occurs, thus precluding shape memory and pseudoelasticity in gold nanowires.

It is expected that variations in the loading rate would have a minimal effects on the deformation mechanisms observed, provided that the strain rate remains below about $\dot{\varepsilon} \approx 10^{10}\,\mathrm{s}^{-1}$ (Ikeda et al., 1999; Branicio and Rino, 2000); previous investigations by Gall et al. (2004) utilizing both dynamic and quasistatic loading of nanowires found little difference in the response observed between the two loading conditions. In addition, the underestimation of the surface energies by the EAM potentials should not affect the deformation mechanisms predicted; because the EAM potentials correctly predict that {1 1 0} surfaces have the highest energy, followed by {1 0 0} and {1 1 1}, only quantitative errors, such as exact predictions of the stress–strain response or yield strains should be introduced.

In closing, we note that recent analytical predictions of twinnability, or the propensity of a material to form twins rather than partial dislocations, in FCC materials have been made by Tadmor and Bernstein (2004) and Bernstein and Tadmor (2004), who used an energetic comparison similar to that made originally by Rice (1992) to study whether deformation twinning or dislocation nucleation would occur at a crack tip. While their analysis is elegant and leads to a closed form analytical expression for twinnability, their model is valid for polycrystalline materials loaded in quasistatic tension at zero temperature. The

results of the present study indicate that any future analytic predictions of deformation mode in nanomaterials, including the Schmid factor analysis used here for qualitative comparisons and that of Tadmor and Bernstein, must include wire orientation, loading condition and transverse free surface orientation.

5. Conclusions

In conclusion, we have studied the fundamental deformation mechanisms in various single crystal metal nanowires with different orientations deformed under tension and compression; the findings are summarized in Fig. 13. The key finding of this paper is the direct, first order effect that side surface orientation can have on the operant deformation mode seen in the nanowires. The importance of free surfaces was illustrated in nanowires with two different normal orientations, ⟨1 0 0⟩ and ⟨1 1 0⟩, and various side surface orientations.

For the ⟨1 1 0⟩ wires, low energy {1 1 1} side surfaces prevented free-surface initiated slip during compressive loading, in contrast to the slip observed in the ⟨1 1 0⟩ nanowires with higher energy {1 0 0} and {1 1 0} side surfaces. For the ⟨1 0 0⟩ wires, simple rotation of the crystal orientation about its longitudinal axis alters the deformation mode from twinning for the ⟨1 0 0⟩/{1 0 0} wires to distributed stacking faults for the ⟨1 0 0⟩/{1 1 0} wires. We reemphasize that the ability to completely alter the operant deformation mechanisms in a material via rotation about its uniaxial deformation direction is a unique effect in nanometer scale materials that does not occur in bulk solids.

The results obtained in this work shed light on the crucial factors which must be incorporated into predictive models of deformation (Karaman et al., 2001a, b; Tadmor and Bernstein, 2004; Bernstein and Tadmor, 2004) in nanomaterials or should be studied

Orientation	Loading	Predicted	Observed
<100>/{100}	Tension	Slip	Partial dislocations
<100>/{100}	Compression	Twin	Twin
<100>/{110}	Compression	Twin	Partial dislocations
<110>	Tension	Twin	Partial dislocations
<110>/{111}	Tension	Twin	Twin
<110>	Compression	Slip	Full and partial dislocations
<110>/{111}	Compression	Slip	No line defects

Fig. 13. Summary of predicted and observed deformation mechanisms for the various nanowire orientations and loading conditions.

in emerging experimental studies of nanowire deformation. In particular, these factors must account for the free surface orientation and structure to accurately predict the deformation patterns at the nanoscale. The simulation results shown in this paper indicate that until fully analytical predictions of material deformation can be made, atomistic simulations will continue to be necessary to predict and understand deformation patterns in nanometer scale metals.

While definitive progress in understanding nanoscale deformation mechanisms and their causes has been achieved in this work, there still remain important and unresolved issues. For example, the sensitivity of the observed deformation mechanisms to factors such as pre-existing defects, vacancies, variations in orientation should be quantified to make contact with nanoscale mechanical experiments. In addition, it will be important to determine whether effects such as cross sectional geometry, aspects ratios of the nanowires, or nanowire cross sectional size play a role in altering the observed deformation mechanisms. These issues are especially pertinent in determining if there exist crossover sizes at which certain deformation mechanisms can be suppressed or allowed, and will be addressed in future research.

Acknowledgments

HSP gratefully acknowledges startup funding from Vanderbilt University in support of this research. We would also like to thank E. Dave Reedy and Neville R. Moody for their support of this research, and Gregory J. Wagner for his assistance with using the Warp code. Sandia is a multiprogram laboratory operated by Sandia Corporation, a Lockheed Martin Company, for the United States Department of Energy's National Nuclear Security Administration under contract DE-AC04-94AL85000.

References

Angelo, J.E., Moody, N.R., Baskes, M.I., 1995. Trapping of hydrogen to lattice defects in nickel. Modelling Simulation Mater. Sci. Eng. 3, 289–307.

Bernstein, N., Tadmor, E.B., 2004. Tight-binding calculations of stacking energies and twinnability in FCC metals. Phys. Rev. B 69, 094116.

Brandbyge, M., Schiotz, J., Sorensen, M.R., Stoltze, P., Jacobsen, K.W., Norskov, J.K., Olesen, L., Laegsgaard, E., Stensgaard, I., Besenbacher, F., 1995. Quantized conductance in atom-sized wires between two metals. Phys. Rev. B 52 (11), 8499–8514.

Branicio, P.S., Rino, J.P., 2000. Large deformation and amorphization or Ni nanowires under uniaxial strain: a molecular dynamics study. Phys. Rev. B 62 (24), 16950–16955.

Chen, M., Ma, E., Hemker, K.J., Sheng, H., Wang, Y., Cheng, X., 2003. Deformation twinning in nanocrystalline aluminum. Science 300, 1275–1277.

Christian, J.W., Mahajan, S., 1995. Deformation twinning. Progr. Mater. Sci. 39, 1–157.

Coura, P.Z., Legoas, S.G., Moreira, A.S., Sato, F., Rodrigues, V., Dantas, S.O., Ugarte, D., Galvao, D.S., 2004. On the structural and stability features of linear atomic suspended chains formed from gold nanowires stretching. Nano Lett. 4 (7), 1187–1191.

da Silva, E.Z., da Silva, A.J.R., Fazzio, A., 2001. How do gold nanowires break? Phys. Rev. Lett. 87 (25), 256102.

Daw, M.S., Baskes, M.I., 1984. Embedded-atom method: derivation and application to impurities, surfaces, and other defects in metals. Phys. Rev. B 29 (12), 6443–6453.

Diao, J., Gall, K., Dunn, M.L., 2003. Surface-stress-induced phase transformation in metal nanowires. Nature Mater. 2 (10), 656–660.

Diao, J., Gall, K., Dunn, M.L., 2004. Yield asymmetry in metal nanowires. Nano Lett. 4 (10), 1863–1867.

El-Danaf, E., Kalidindi, S.R., Doherty, R.G., 1999. Influence of grain size and stacking-fault energy on deformation twinning in FCC metals. Metall. Mater. Trans. A 30A, 1223–1233.

Foiles, S.M., Baskes, M.L., Daw, M.S., 1986. Embedded-atom-method functions for the FCC metals Cu, Ag, Au, Ni, Pd, Pt and their alloys. Phys. Rev. B 33 (12), 7893–7991.

Gall, K., Diao, J., Dunn, M.L., 2004. The strength of gold nanowires. Nano Lett. 4 (12), 2431–2436.

Gall, K., Diao, J., Dunn, M.L., Haftel, M., Bernstein, N., Mehl, M.J., 2005. Tetragonal phase transformation in gold nanowires. J. Eng. Mater. Technol. 127, 417–422.

Gulseren, O., Ercolessi, F., Tosatti, E., 1998. Noncrystalline structures of ultrathin unsupported nanowires. Phys. Rev. Lett. 80 (17), 3775–3778.

Hirthe, J.P., Lothe, J., 1982. Theory of Dislocations, second ed. Krieger Publishing Company, Malabar, FL.

Hoover, W.G., 1985. Canonical dynamics: equilibrium phase-space distributions. Phys. Rev. A 31, 1695–1697.

Horstemeyer, M.F., Hamilton, J.C., Thompson, A., Baskes, M.I., Plimpton, S.J., Daruka, I., Sorenson, M.R., Voter, A.F., Ford, D.M., Rallabandi, P.S., Tunca, C. From atom-picoseconds to centimeter-years in simulation and experiment. Sandia Technical Report SAND2001-81 1 1.

Ikeda, H., Qi, Y., Cagin, T., Samwer, K., Johnson, W.L., III, W.A.G., 1999. Strain rate induced amorphization in metallic nanowires. Phys. Rev. Lett. 82 (14), 2900–2903.

Jagla, E.A., Tosatti, E., 2001. Structure and evolution of a metallic nanowire-tip junction. Phys. Rev. B 64, 205412.

Karaman, I., Sehitoglu, H., Gall, K., Chumlyakov, Y.I., Maier, H.J., 2000. Deformation of single crystal hadfield steel by twinning and slip. Acta Materialia 48 (6), 1345–1359.

Karaman, I., Sehitoglu, H., Chumlyakov, Y.I., Maier, H.J., Kireeva, I.V., 2001a. The effect of twinning and localized slip on the bauschinger effect of hadfield steel single crystals. Metall. Mater. Trans. A 32A, 695–706.

Karaman, I., Sehitoglu, H., Chumlyakov, Y.I., Maier, H.J., Kireeva, I.V., 2001b. Extrinsic stacking faults and twinning in hadfield manganese steel single crystals. Scripta Materialia 44, 337–343.

Kelchner, C.L., Plimpton, S.J., Hamilton, J.C., 1998. Dislocation nucleation and defect structure during surface indentation. Phys. Rev. B 58 (17), 11085–11088.

Kondo, Y., Takayanagi, K., 1997. Gold nanobridge stabilized by surface structure. Phys. Rev. Lett. 79 (18), 3455–3458.

Kondo, Y., Takayanagi, K., 2000. Synthesis and characterization of helical multi-shell gold nanowires. Science 289, 606–608.

Landman, U., Luedtke, W.D., Burnham, N.A., Colton, R.J., 1990. Atomistic mechanisms and dynamics of adhesion, nanoindentation, and fracture. Science 248, 454–461.

Liang, W., Zhou, M., 2004. Response of copper nanowires in dynamic tensile deformation. Proc. Inst. Mech. Eng., Part C: J. Mech. Eng. Sci. 218 (6), 599–606.

Liang, M., Zhou, W., 2005. Pseudoelasticity of single crystalline Cu nanowires through reversible lattice reorientations. J. Eng. Mater. Technol. 127 (4), 423–433.

Liang, W., Zhou, M., Ke, F., 2005. Shape memory effect in Cu nanowires. Nano Lett. 5 (10), 2039–2043.

Lieber, C.M., 2003. Nanoscale science and technology: building a big future from small things. MRS Bull. 28 (7), 486–491.

Liu, Z., Yang, Y., Liang, J., Hu, Z., Li, S., Peng, S., Qian, Y., 2003. Synthesis of copper nanowires via complex-surfactant-assisted hydrothermal reduction process. J. Phys. Chem. B 107, 12658–12661.

Mehrez, H., Ciraci, S., 1997. Yielding and fracture mechanisms of nanowires. Phys. Rev. B 56 (19), 12632–12642.

Meyers, M.A., Benson, D.J., Vohringer, O., Kad, B.K., Xue, Q., Fu, H.H., 2002. Constitutive description of dynamic deformation: physically-based mechanisms. Mater. Sci. Eng. A 322, 194–216.

Nosé, S., 1984. A unified formulation of the constant temperature molecular dynamics methods. J. Chem. Phys. 81, 511–519.

Ohnishi, H., Kondo, Y., Takayanagi, K., 1998. Quantized conductance through individual rows of suspended gold atoms. Nature 395, 780–783.

Park, H.S., 2006. Stress-induced martensitic phase transformation in intermetallic nickel aluminum nanowires. Nano Lett., accepted for publication.

Park, H.S., Ji, C., On the thermomechanical deformation of silver shape memory nanowires, Acta Materialia, accepted for publication.

Park, H.S., Zimmerman, J.A., 2005. Modeling inelasticity and failure in gold nanowires. Phys. Rev. B 72, 054106.

Park, H.S., Zimmerman, J.A., 2006. Stable nanobridge formation in ⟨1 1 0⟩ gold nanowires under tensile deformation. Scripta Materialia 54, 1127–1132.

Park, H.S., Gall, K., Zimmerman, J.A., 2005. Shape memory and pseudoelasticity in metal nanowires. Phys. Rev. Lett. 95, 255504.

Plimpton, S.J., 1995. Fast parallel algorithms for short-range molecular dynamics. J. Comput. Phys. 117, 1–19.

Rice, J.R., 1992. Dislocation nucleation from a crack tip: an analysis based on the peierls concept. J. Mech. Phys. Solids 40 (2), 239–271.

Rodrigues, V., Fuhrer, T., Ugarte, D., 2000. Signature of atomic structure in the quantum conductance of gold nanowires. Phys. Rev. Lett. 85 (19), 4124–4127.

Sanchez-Portal, D., Artacho, E., Junquera, J., Ordejon, P., Garcia, A., Soler, J.M., 1999. Stiff monoatomic gold wires with a spinning zigzag geometry. Phys. Rev. Lett. 83 (19), 3884–3887.

Shenoy, V.B., 2005. Atomistic calculations of elastic properties of metallic FCC crystal surfaces. Phys. Rev. B 71, 094104.

Tadmor, E.B., Bernstein, N., 2004. A first principles measure for the twinnability of FCC metals. J. Mech. Phys. Solids 52, 2507–2519.

Torres, J.A., Tosatti, E., Corso, A.D., Ercolessi, F., Kohanoff, J.J., Tolla, F.D.D., Soler, J.M., 1999. The puzzling stability of monoatomic gold wires. Surf. Sci. Lett. 426, L441–L446.

Vitos, L., Ruban, A.V., Skriver, H.L., Kollar, J., 1998. The surface energy of metals. Surf. Sci. 411, 186–202.

Walsh, P., Li, W., Kalia, R.K., Nakano, A., Vashista, P., Saini, S., 2001. Structural transformation, amorphization, and fracture in nanowires: a multimillion-atom molecular dynamics study. Appl. Phys. Lett. 78 (21), 3328–3330.

Wan, J., Fan, Y.L., Gong, D.W., Shen, S.G., Fan, X.Q., 1999. Surface relaxation and stress of FCC metals: Cu, Ag, Au, Ni, Pd, Pt, Al and Pb. Modelling Simulation Mater. Sci. Eng. 7, 189–206.

Warp. ⟨http://www.cs.sandia.gov/~sjplimp/lammps.html⟩.

Wu, H.A., Soh, A.K., Wang, X.X., Sun, Z.H., 2004. Strength and fracture of single crystal metal nanowire. Key Eng. Mater. 261–263, 33–38.

Yang, P., 2005. The chemistry and physics of semiconductor nanowires. MRS Bull. 30 (2), 85–91.

Zimmerman, J.A., Gao, H., Abraham, F.F., 2000. Generalized stacking fault energies for embedded atom FCC metals. Modelling Simulation Mater. Sci. Eng. 8, 103–115.